

Hadron Resonance Gas Model for An Arbitrarily Large Number of Different Hard-Core Radii

K. A. Bugaev^{1*}, V. V. Sagun^{1,2}, A. I. Ivanytskyi¹, I. P. Yakimenko³, E. G. Nikonov⁴, A.V. Taranenko⁵ and G. M. Zinovjev¹

¹*Bogolyubov Institute for Theoretical Physics, Metrologichna str. 14^B, Kiev 03680, Ukraine*

²*CENTRA, Instituto Superior Técnico, Universidade de Lisboa, Av. Rovisco Pais 1, 1049-001 Lisboa, Portugal*

³*Department of Physics, Chemistry and Biology (IFM), Linköping University, SE-58183 Linköping, Sweden*

⁴*Laboratory for Information Technologies, JINR, Joliot-Curie str. 6, 141980 Dubna, Russia*

⁵*National Research Nuclear University “MEPhI” (Moscow Engineering Physics Institute), Kashirskoe Shosse 31, 115409 Moscow, Russia*

* *E-mail: Bugaev@th.physik.uni-frankfurt.de*

Abstract

We develop a novel formulation of the hadron-resonance gas model which, besides a hard-core repulsion, explicitly accounts for the surface tension induced by the interaction between the particles. Such an equation of state allows us to go beyond the Van der Waals approximation for any number of different hard-core radii. A comparison with the Carnahan-Starling equation of state shows that the new model is valid for packing fractions 0.2-0.22, while the usual Van der Waals model is inapplicable at packing fractions above 0.1-0.11. Moreover, it is shown that the equation of state with induced surface tension is softer than the one of hard spheres and remains causal at higher particle densities. The great advantage of our model is that there are only two equations to be solved and it does not depend on the various values of the hard-core radii used for different hadronic resonances. Using this novel equation of state we obtain a high-quality fit of the ALICE hadron multiplicities measured at center-of-mass energies of 2.76 TeV per nucleon. Furthermore, using the traditional hadron-resonance gas model with multi-component hard-core repulsion and the novel one we investigate the recently suggested model in which the proper volume of a hadron is proportional to its mass. We find that the high-temperature maximum of χ^2/ndf observed in the latter model always appears in the region located far above the limit of its applicability.

1 Introduction

During the last few years the hadron-resonance gas model (HRGM) [1] became a precise and reliable tool to extract the parameters of chemical freeze-out (CFO). The traditional versions of the HRGM are basically the Van der Waals equation of state (EOS) which is formulated for all hadrons and hadronic resonances and which employs either one hard-core radius R for all hadrons, or at least two hard-core radii: one for mesons R_m and one for baryons R_B . However, the main achievements in this field come from a formulation of the HRGM with multi-component hard-core repulsion (MHRGM) [2, 3, 4, 5]. At the moment, the MHRGM contains at most five different hard-core radii: the pion hard-core radius R_π , the kaon hard-core radius R_K , the hard-core radius of Λ -(anti)hyperons in addition to the ones for other baryons R_B and for other mesons R_m . Having introduced four hard-core radii (no radius for Λ -(anti)hyperons) it was possible for the first time to describe the Strangeness Horn [2] with the highest quality $\chi^2/ndf \simeq 7.3/14$ and at the same time successfully fit 111 independent hadron multiplicities ratios measured from AGS ($\sqrt{s_{NN}} = 2.7$ GeV) to top RHIC ($\sqrt{s_{NN}} = 200$ GeV) collision energies with the fit quality $\chi^2/ndf \simeq 1.16$, which was the best result at that time.

A couple of years later, taking into account one more global fitting parameter – namely the hard-core radius of Λ -(anti)hyperons, which turned out to be a very influential parameter – it was possible to

decrease the value of χ^2/ndf by about 20 percent and to reach the best fit quality of these data which is $\chi^2/ndf \simeq 0.95$ [5]. Furthermore, the developed MHRGM allowed one to formulate the concept of separate CFOs of strange and non-strange hadrons [3, 6], which naturally explains the apparent chemical non-equilibrium of strange charge in nucleus-nucleus collisions. And last but not least, the very high quality description of data allowed us to study the thermodynamics at CFO with very high confidence and to find novel irregularities and signals of mixed-phase formation in nuclear collisions [4, 7].

In view of future experiments at the NICA-JINR and FAIR-GSI accelerators we expect to obtain much more experimental data with a substantially higher accuracy. Evidently, these new data will, hopefully, allow us to study the second virial coefficients of the most abundant (or maybe even those of all measured) hadrons. For such a task a MHRGM with many hard-core radii should be formulated. However, since the existing MHRGM for N different hard-core radii requires the knowledge of a solution of N transcendental equations, a further increase of the number of hard-core radii (i.e., $N \sim 100$, corresponding to the various hadronic species created in a collision) will lead to a substantial increase of computational time and will destroy the main attractive feature of the thermal model, i.e., its simplicity.

Recently, there appeared a work [8] in which the authors suggested to use the relation $V_h = C \cdot m_h$ between the hadronic proper volume V_h and its mass m_h . However, the authors of Ref. [8] applied the Van der Waals approximation, which rapidly becomes invalid when the hard-core radii become too large. Since the issues raised in Ref. [8] are very important for heavy-ion phenomenology, we would like to re-analyse ALICE data [9, 10, 11, 12, 13, 14, 15] with the conventional MHRGM and with the novel model, which is able to go beyond the usual Van der Waals approximation.

For this purpose, we present here an entirely new version of the HRGM with multi-component hard-core repulsion: The Van der Waals EOS with induced surface tension (abbreviated IST EOS in the following). The IST EOS is based on the virial expansion for a multi-component mixture and, hence, it naturally switches between the low- and high-density limit. Comparing it to the Carnahan-Starling EOS [16] for one and two particle species we find an almost perfect agreement between them up to packing fractions $\eta \simeq 0.2 - 0.22$. Its great advantage is that, independent from the number of different hard-core radii, the IST EOS only involves solving a system of two transcendental equations. Using the IST EOS we successfully fit the ALICE data [9, 10, 11, 12, 13, 14, 15] and compare the obtained results with the results found by the MHRGM as well as by the model of Ref. [8].

This paper is organized as follows: in the next section we present the main features of the IST EOS; in Sec. 3 the fit of the ALICE data by different versions of the HRGM is described in detail; Sec. 4 is devoted to a thorough analysis of the applicability bounds of various versions of the HRGM, including the Vovchenko-Stoecker model [8]; the discussion of results is given in Sec. 5; our conclusions are formulated in Sec. 6, and the Appendix contains useful formulae.

2 HRGM with the induced surface tension

In order to use an arbitrarily large number of independent hard-core radii, we employ the IST EOS which is much more effective compared to the traditional MHRGM [2, 3, 4, 5]. Such a model was derived on the basis of the virial expansion for a multi-component mixture [17] obtained for the simplified statistical multifragmentation model [18] with an infinite number of hard-core radii of nuclear fragments of all sizes. The thermodynamically consistent equation of state developed in Ref. [17] is a system of coupled equations for the pressure p and the induced surface-tension coefficient Σ . Applying it to the pressure and the induced surface-tension coefficient of the hadron-resonance gas, we obtain

$$p = T \sum_{k=1}^N \phi_k \exp \left[\frac{\mu_k}{T} - \frac{4}{3} \pi R_k^3 \frac{p}{T} - 4 \pi R_k^2 \frac{\Sigma}{T} \right], \quad (1)$$

$$\Sigma = T \sum_{k=1}^N R_k \phi_k \exp \left[\frac{\mu_k}{T} - \frac{4}{3} \pi R_k^3 \frac{p}{T} - 4 \pi R_k^2 \alpha \frac{\Sigma}{T} \right], \quad (2)$$

$$\mu_k = \mu_B B_k + \mu_{I3} I_{3k} + \mu_S S_k, \quad (3)$$

where μ_B , μ_S , μ_{I3} are the baryonic, the strange, and the third projection of the isospin chemical potential, respectively. Here B_k , S_k , I_{3k} , m_k and R_k denote, respectively, the corresponding charges, mass, and hard-core radius of the k -th hadronic species. The sums in Eqs. (1) and (2) run over all hadronic species; their corresponding antiparticles are considered as independent species.

The one-particle thermal density ϕ_k in Eqs. (1) and (2) accounts for the Breit-Wigner mass attenuation and is written in the Boltzmann approximation

$$\phi_k = g_k \gamma_S^{|s_k|} \int_{M_k^{Th}}^{\infty} \frac{dm}{N_k(M_k^{Th})} \frac{1}{(m - m_k)^2 + \Gamma_k^2/4} \int \frac{d^3p}{(2\pi)^3} \exp \left[-\frac{\sqrt{p^2 + m^2}}{T} \right], \quad (4)$$

where g_k is the degeneracy factor of the k -th hadronic species, γ_S is the strangeness suppression factor [20], $|s_k|$ is the number of valence strange quarks and antiquarks in this hadron species, $N_k(M_k^{Th}) \equiv \int_{M_k^{Th}}^{\infty} \frac{dm}{(m - m_k)^2 + \Gamma_k^2/4}$ denotes a normalization factor, while M_k^{Th} corresponds to the decay threshold mass of the k -th hadronic species.

To study nuclear collisions the system of Eqs. (1), (2), and (3) should be supplemented by the strange-charge conservation law

$$\phi_k S_k \exp \left[\frac{\mu_k}{T} - \frac{4}{3} \pi R_k^3 \frac{p}{T} - 4\pi R_k^2 \frac{\Sigma}{T} \right] = 0, \quad (5)$$

which completes the system of equations of the IST EOS.

The dimensionless parameter $\alpha > 1$ is introduced in Eq. (2) due to the freedom of the Van der Waals extrapolation to high densities [17]. As it is shown below, the parameter α makes the Van der Waals EOS more realistic in the high-density limit. In principle, α can be a regular function of T and μ , however, for the sake of simplicity it is fixed to a constant value. In the work [17] it was established that the parameter α should obey the inequality $\alpha > 1$ in order to reproduce the physically correct phase-diagram properties of nuclear matter.

The physical meaning of α can be revealed, if we use the following relation

$$\Sigma_k = p_k R_k \exp \left[-4\pi R_k^2 \cdot (\alpha - 1) \frac{\Sigma}{T} \right], \quad (6)$$

between the partial pressure p_k of the k -th hadronic species and the corresponding partial induced surface-tension coefficient Σ_k . The system pressure $p = \sum_{k=1}^N p_k$ and the total induced surface-d tension coefficient $\Sigma = \sum_{k=1}^N \Sigma_k$ are the sums of their corresponding partial values.

In the next paragraph, for the sake of simplicity, we assume that all particles have the same hard-core radius $R_k = \tilde{R}$ for $k = 1, 2, 3, \dots$ and, consequently, the same proper volume \tilde{v} . Using Eq. (6) one can identically rewrite Eq. (1) in the form

$$\begin{aligned} p &= T \sum_{k=1}^N \phi_k \exp \left[\frac{\mu_k}{T} - \tilde{v} \frac{p}{T} - 3\tilde{v} \frac{p}{T} \cdot \exp \left[-3\tilde{v} \cdot (\alpha - 1) \frac{\Sigma}{T \tilde{R}} \right] \right] \\ &= T \sum_{k=1}^N \phi_k \exp \left[\frac{\mu_k}{T} - v^{eff} \frac{p}{T} \right], \end{aligned} \quad (7)$$

where we introduce the effective excluded volume of hadrons of species k

$$v^{eff} = \tilde{v} \left[1 + 3 \cdot \exp \left[-3\tilde{v} \cdot (\alpha - 1) \frac{\Sigma}{T \tilde{R}} \right] \right]. \quad (8)$$

The low-density limit is obtained for $\mu_k \rightarrow -\infty$. In this limit $\frac{\Sigma \tilde{v}}{T \tilde{R}} \rightarrow 0$ and, hence, $v^{eff} \simeq 4\tilde{v}$, i.e., it correctly reproduces the excluded volume for the one-component case. In the high-density limit $\frac{\Sigma \tilde{v}}{T \tilde{R}} \gg 1$,

since $\mu_k/T \gg 1$. Therefore, for $\alpha > 1$ the exponential function on the right-hand side of Eq. (8) vanishes and the effective excluded volume becomes equal to the proper volume, i.e., $v^{eff} \simeq \tilde{v}$. Thus, in the present model the parameter α switches between the excluded-volume and the proper-volume regimes. In order to apply this equation of state to describe the hadron multiplicities we have to fix the value of α . For this purpose we compare the one-component system of equations of state (1), (2) with the famous one-component Carnahan-Starling (CS) EOS [16],

$$P = \rho T Z_{CS}, \quad Z_{CS} = \frac{1 + \eta + \eta^2 - \eta^3}{(1 - \eta)^3}. \quad (9)$$

The CS EOS is more accurate at higher densities than the excluded-volume model (EVM), which is a more proper name for the Van der Waals EOS with repulsion. Here the packing fraction of particles of the same hard-core radius R is $\eta = \frac{4}{3}\pi R^3 \rho$, where ρ is their particle density. From Fig. 1 one can see that up to $\eta \simeq 0.22$ the IST EOS with $\alpha = 1.25$ reproduces both the compressibility factor Z and the speed of sound c_s of the CS EOS. Figure 1 represents an extreme case, when the pion hard-core radius is set to zero, while the baryons (here, nucleons and $\Delta_{P33}(1232)$ isobars were accounted for) have a rather large radius $R_B = 0.4$ fm, and additionally it corresponds to an unphysically high temperature $T = 200$ MeV. To include point-like pions, we added the ideal pion-gas pressure to the baryonic pressure given by Eq. (9) according to Ref. [19]. Therefore, the value $\alpha = 1.25$ is used in the present work.

We have to note that for pions we used the Bose-Einstein distribution function

$$\phi_\pi = g_\pi \int \frac{d^3p}{(2\pi)^3} \frac{1}{\exp\left[\frac{\sqrt{p^2 + m_\pi^2}}{T}\right] - 1}, \quad (10)$$

instead of Eq. (4) because at high temperatures the quantum correction cannot be ignored. In principle, one would need the quantum generalization of the system (1), (2), but the fit of ALICE data corresponds to vanishing values of all chemical potentials. In addition, the pion hard-core radius is rather small compared to other mesons, therefore, for the sake of simplicity, in Eqs. (1), (2), and (3) we used Eq. (10) instead of the Boltzmann approximation (4).

It is worth noting that the traditional EVM, i.e., the Van der Waals EOS, corresponds to the case $\alpha = 1$. From Fig. 1 one can see that such an EOS is in agreement with the CS EOS up to a packing fraction $\eta \simeq 0.1 - 0.11$ only. Also from this figure it is clearly seen that the EVM violates causality at a baryonic density of about 0.64 fm^{-3} ($\eta \simeq 0.17$), while the IST EOS remains causal for baryonic densities above 1 fm^{-3} . Such an advantage of the IST EOS is of principal importance for hydrodynamic simulations.

Using the value $\alpha = 1.25$ we employed the IST EOS to fit the independent hadronic-multiplicity ratios [21] measured in central nuclear collisions for center-of-mass energies $\sqrt{s_{NN}} = 2.7, 3.3, 3.8, 4.3, 4.9, 6.3, 7.6, 8.8, 9.2, 12, 17, 62.4, 130, \text{ and } 200 \text{ GeV}$ (for details see Ref. [2, 3, 5]). Then we compared the obtained results with the ones from the MHRGM with hard-core radii found in Ref. [5], i.e., for the hard-core radii of baryons $R_b = 0.355$ fm, mesons $R_m = 0.4$ fm, pions $R_\pi = 0.1$ fm, kaons $R_K = 0.395$ fm, and Λ hyperons $R_\Lambda = 0.11$ fm. Treating γ_S as a fitting parameter in the IST EOS we found that the best data description of the same data set which was used in Ref. [5] corresponds to the following values of hard-core radii (new radii hereafter) of baryons $R_b = 0.365$ fm, mesons $R_m = 0.42$ fm, pions $R_\pi = 0.15$ fm, kaons $R_K = 0.395$ fm, and Λ hyperons $R_\Lambda = 0.085$ fm. These values of the hard-core radii generate $\chi^2/ndf = 57.099/55 \simeq 1.038$ which is about 9% larger than the χ^2/ndf found earlier in Ref. [5] for the EVM. Hence, in the present work we use exactly this new set of hard-core radii for the analysis of the ALICE data.

Compared to the values found by the MHRGM, one sees that only the pion hard-core radius increased by 50%, while the hard-core radius of Λ hyperons diminished by 20%. The most important thing is that these radii remain essentially smaller than R_b , R_m , and R_K . The latter hard-core radii are practically unchanged. The most prominent changes of the fit are compared in Fig. 2 with the corresponding values from Ref. [5]. As one can see from this figure, at the center-of-mass energy $\sqrt{s_{NN}} = 6.3 \text{ GeV}$ only the ratio K^-/K^+ is essentially improved, while for $\sqrt{s_{NN}} = 130 \text{ GeV}$ the ratios K^+/π^+ , \bar{p}/π^- , Ω/π^- , and ϕ/K^- are described better than within the MHRGM. The fit results obtained by the MHRGM and by the IST EOS for the other collision energies are hardly distinguishable from each other.

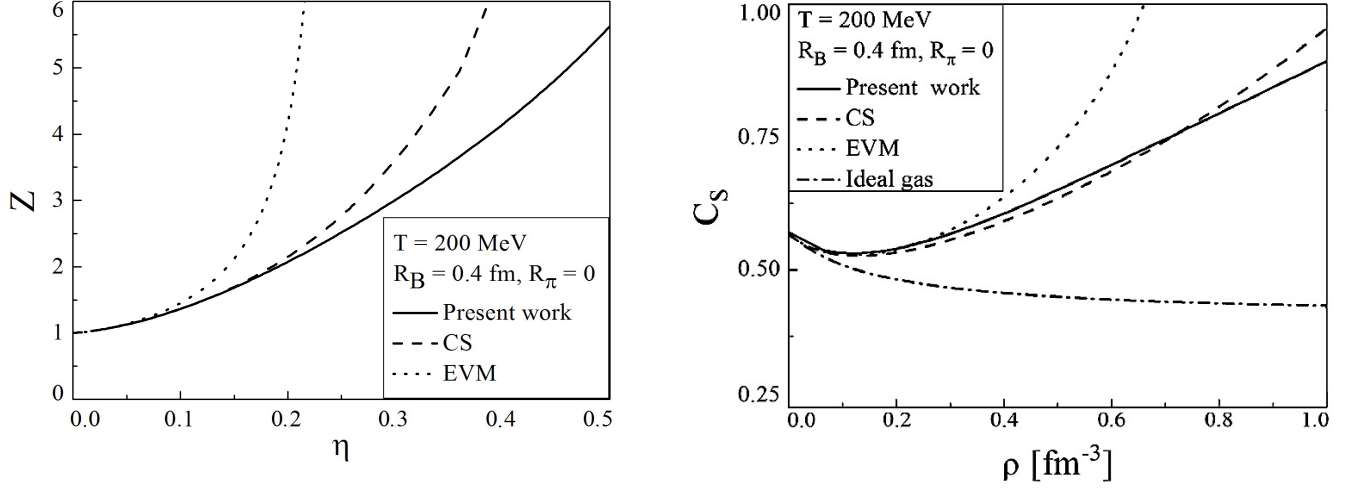


Figure 1: **Left panel:** The compressibility factor Z of a gas consisting of point-like pions and baryons (nucleons and $\Delta_{P33}(1232)$ isobars were accounted for) with a hard-core radius of 0.4 fm is shown for different EOS as a function of baryon packing fraction η . The Van der Waals EOS (dotted curve), the IST EOS (solid curve), and the CS EOS (long dashed curve) are shown for $T = 200 \text{ MeV}$. **Right panel:** The speed of sound as a function of baryonic density is shown for the same EOS as in the left panel and with the same notations. The dotted-dashed curves shows the speed of sound of point-like pions and baryons.

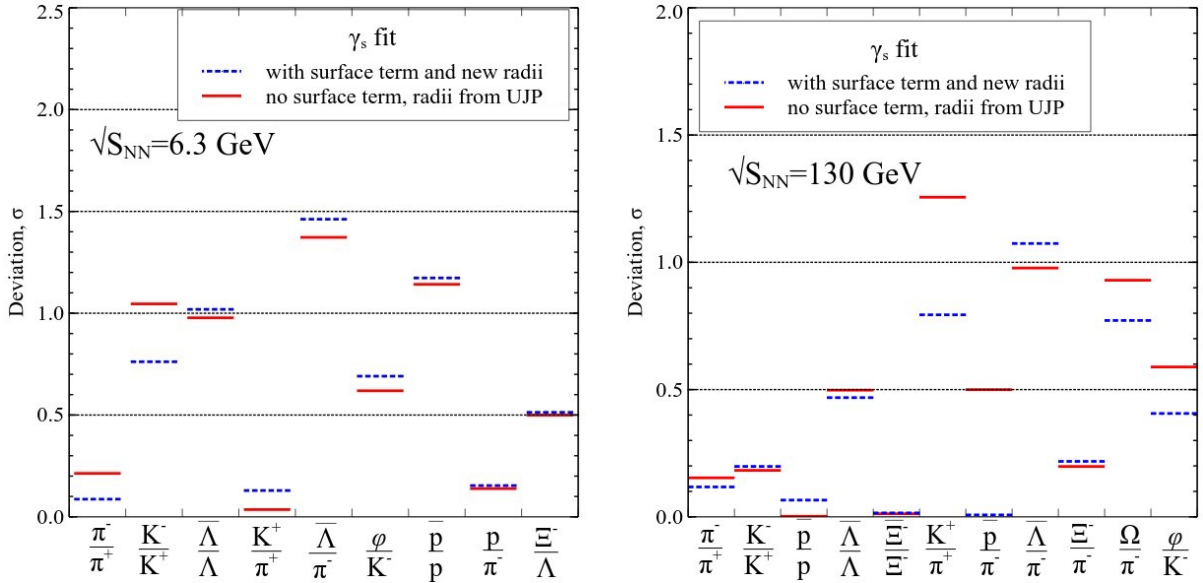


Figure 2: (Color online) Deviation of theoretically predicted hadronic ratios from experimental values in units of experimental error σ for $\sqrt{s_{NN}} = 6.3 \text{ GeV}$ (left panel) and $\sqrt{s_{NN}} = 130 \text{ GeV}$ (right panel). Solid lines correspond to the original MHRGM with γ_s fit [5], while dashed lines correspond to the IST EOS fit with the γ_s parameter [21].

3 Hadron-Multiplicity Data of the ALICE Experiment

The data to be fitted are the hadron multiplicities at midrapidity $\frac{dN}{dy}|_{|y|<0.5}$, measured by the ALICE detector at $\sqrt{s_{NN}} = 2.76$ TeV in Pb + Pb collisions. All of them are p_T -integrated. The detector cannot measure particles at low p_T ; as a result, the multiplicities have to be extrapolated. The extrapolation was performed by a blast-wave fit in each centrality bin; the extrapolation error is included in the systematic errors. Thus, all the following data are from the same kinematic region.

In general we are interested in the most central collisions. However, the experimental centrality bins are different for different particles. If there is enough statistics there are more bins; whereas for the rare particles there are less bins and the bins are larger. In some cases the hadron multiplicity does not depend on centrality, but for most hadron species one has to be very careful with the centrality selection. Simultaneous fitting of, e.g. the π multiplicity at 0-5% centrality, Ξ at 0-10% centrality, and ${}^3\text{He}$ at 0-20% centrality, is not acceptable if one aims at a precise description of the data. On the other hand, the multiplicity ratios (with corresponding centrality bins) seem to be independent of centrality. Therefore, first we give a table of raw experimental data from publications (see Table 1) and then a table of quantities which we used for a subsequent analysis (Table 2). Our experience tells us that, besides the numerical convenience, fitting the ratios of hadron yields provides a better stability of the results.

Similarly to Ref. [22] we do not include the K^* data into the fitting procedure. The K^* yield is known to have around 3σ deviation from the thermal-model prediction, and it is not included to fit the thermal parameters in recent works (see caption of Fig. 1 in Ref. [22]), because “as a strongly decaying resonance its yield can be significantly modified after chemical freeze-out” [22]. We agree with this argument, since the reactions like $K + \pi \leftrightarrow K^*$ can occur after chemical freeze-out and change the K^* yields. Due to a technical reason we do not fit the K_S^0 data. As one can see from Table 1 the multiplicity of K_S^0 meson is identical to the ones of K^+ and K^- mesons. Since in our fit all chemical potentials are fixed to zero (see below), then the K_S^0 meson is formally indistinguishable from K^+ and K^- mesons and because of this fact any ratio involving K_S^0 meson is not independent. Therefore, it is omitted from the fit.

Hence, overall we have 19 hadron species to fit (π^\pm , K^\pm , p , \bar{p} , ϕ , Λ , Ξ^\pm , Ω^\pm , d , \bar{d} , ${}^3\text{He}$, ${}^3\overline{\text{He}}$, ${}^4\overline{\text{He}}$, ${}^3_\Lambda\text{H}$, ${}^3_\Lambda\overline{\text{H}}$), or 18 ratios, respectively. In Ref. [22] the centrality is 0-10% for all species, but in Refs. [9, 10, 11, 12, 13, 14, 15] such a centrality class is not always present, as one can see from Table 1. Fortunately, the multiplicity ratios are rather independent on centrality – if the same centrality class is taken for numerator and denominator. Consequently, we take such ratios for our fit. To obtain the 0-10% centrality class from the 0-5% and 5-10% classes we take the average value of the corresponding multiplicities and the average values of the errors. Apparently, this can be done under assumption that the relative experimental error of dN/dy is independent of centrality, which is approximately true for the ALICE data. Therefore, constructing the ratio $r = \frac{A}{B}$ from species $A + \Delta A$ and $B + \Delta B$, we estimate a relative error $\epsilon_r \equiv \frac{\Delta r}{r}$ as $\sqrt{\epsilon_A^2 + \epsilon_B^2}$ [23], where $\epsilon_A = \frac{\Delta A}{A}$ and $\epsilon_B = \frac{\Delta B}{B}$. This is certainly overestimating the error, because a part of the systematic errors, such as errors related to detector acceptance, is usually canceled in the experimentally measured ratios. If statistical and systematic errors ΔA_{stat} and ΔA_{sys} are given, we add them as $\Delta A = \sqrt{\Delta A_{stat}^2 + \Delta A_{sys}^2}$ [23].

As usual, in all our fits of the ALICE data the finite width of resonances is always taken into account according to Eq. (4), while the γ_S parameter [20] is set $\gamma_S = 1$ and all chemical potentials are set to zero. As usual, the total multiplicities are found using the thermal and the decay contributions $n_X^{tot} = n_X^{th} + n_X^{decay} = n_X^{th} + \sum_Y n_Y^{th} Br(Y \rightarrow X)$, where $Br(Y \rightarrow X)$ is the decay branching ratio of the Y-th hadron into the hadron X (for more details see Ref. [5]). The expressions which are necessary to calculate the particle density of hadrons of species k and their charge densities are given in the Appendix.

First we fitted the full set of ALICE data using the MHRGM for the hard-core radii found earlier [5]. From Fig. 3 one can see that the MHRGM describes the data a bit better than the ideal gas (where all hard-core radii are set to zero). It is necessary to note that we did not include five hard-core radii into the number of degrees of freedom since they were not used in the fitting procedure. As one can see from Fig. 3 the non-zero hard-core radii help us to essentially improve the description of the $\frac{K^+}{\pi^+}$ ratio and slightly improve the $\frac{\Lambda}{\pi^+}$ ratio.

	dN/dy or ratio	centrality	Ref.
π^+	$733 \pm 54, 606 \pm 42, 455 \pm 31$	0-5, 5-10, 10-20%	[9]
π^-	$732 \pm 52, 604 \pm 42, 453 \pm 31$	0-5, 5-10, 10-20%	[9]
K^+	$109 \pm 9, 91 \pm 7, 68 \pm 5$	0-5, 5-10, 10-20%	[9]
K^-	$109 \pm 9, 90 \pm 8, 68 \pm 6$	0-5, 5-10, 10-20%	[9]
p	$34 \pm 3, 28 \pm 2, 21 \pm 1.7$	0-5, 5-10, 10-20%	[9]
\bar{p}	$33 \pm 3, 28 \pm 2, 21.1 \pm 1.8$	0-5, 5-10, 10-20%	[9]
Ξ^-	$3.34 \pm 0.06 \pm 0.24, 2.53 \pm 0.04 \pm 0.18$	0-10, 10-20%	[10]
Ξ^+	$3.28 \pm 0.06 \pm 0.23, 2.51 \pm 0.05 \pm 0.18$	0-10, 10-20%	[10]
Ω^-	$0.58 \pm 0.04 \pm 0.09, 0.37 \pm 0.03 \pm 0.06$	0-10, 10-20%	[10]
Ω^+	$0.60 \pm 0.05 \pm 0.09, 0.40 \pm 0.03 \pm 0.06$	0-10, 10-20%	[10]
Λ	$26 \pm 3, 22 \pm 2$	0-5, 5-10%	[11]
K_S^0	$110 \pm 10, 90 \pm 6$	0-5, 5-10%	[11]
$\frac{\phi}{K^-} \times 4$	0.45 ± 0.1	0-10%	[12]
$K^*(892)/K^-$	0.2 ± 0.05	0-10%	[12]
d	$(9.82 \pm 0.04 \pm 1.58) \cdot 10^{-2}$	0-10%	[13]
\bar{d}/d	$0.98 \pm 0.01 \pm 0.13$	0-10%	[13]
${}^3\overline{He}/{}^3He$	$0.83 \pm 0.08 \pm 0.16$	0-20%	[13]
p	26 ± 2.1	0-20%	[14]
d	$(8.71 \pm 0.04 \pm 1.58) \cdot 10^{-2}$	0-20%	[14]
3He	$(2.76 \pm 0.09 \pm 0.62) \cdot 10^{-4}$	0-20%	[14]
${}^4\overline{He}$	$(7.88 \pm 3.03 \pm 2.68) \cdot 10^{-7}$	0-20%	[14]
${}^3_{\Lambda}H$	$(3.86 \pm 0.77 \pm 0.68) \times 10^{-5} \times \text{B.R.}$	0-10%	[15]
${}^3_{\Lambda}\bar{H}$	$(3.47 \pm 0.81 \pm 0.69) \times 10^{-5} \times \text{B.R.}$	0-10%	[15]

Table 1: Collection of $\frac{dN}{dy}$ of hadrons at $\sqrt{s_{NN}} = 2.76$ TeV in Pb + Pb collisions measured by ALICE. If two errors are given, then the first one is statistical, and the second one is systematic. B.R. denotes branching ratio of ${}^3_{\Lambda}H \rightarrow {}^3He + \pi^-$, which is estimated to be 15-35%.

Ratio	Value	Error
π^-/π^+	0.99776	0.10023
K^-/K^+	0.99500	0.11645
\bar{p}/p	0.98387	0.11313
Ξ^-/Ξ^+	1.01829	0.10552
Ω^-/Ω^+	0.96667	0.23371
\bar{d}/d	0.98000	0.13038
${}^3\overline{He}/{}^3He$	0.83000	0.17889
${}^3_{\Lambda}\bar{H}/{}^3_{\Lambda}H$	0.89896	0.36364
ϕ/K^-	0.11250	0.02500
p/π^+	0.04630	0.00500
K^+/π^+	0.14937	0.01605
Λ/π^+	0.03585	0.00453
Ξ^+/π^+	0.00490	0.00050
Ω^+/π^+	0.00090	0.00016
d/p	0.00335	0.00067
${}^3He/d$	0.00317	0.00092
${}^4\overline{He}/{}^3He$	0.00286	0.00207
${}^3_{\Lambda}H/d$	0.00177	0.00086

Table 2: Ratios which are analyzed here.

Similarly to Refs. [22, 24] the MHRGM is able to fit very well the ratios involving (anti)nuclei (see Fig. 3), however, we believe that taking the hard-core radius of (anti)nuclei to be the same as for baryons is not quite correct. The fact that the ideal gas is able to reproduce the ratios involving (anti)nuclei also requires an explanation. Therefore, in the rest of this work we compare the results which include and the ones which exclude the (anti)nuclei ratios into fits of the ALICE data. The latter option is also necessary to qualitatively compare our results with the model [8] which does not include the (anti)nuclei data into a fit. A typical example of the IST EOS fit results without the (anti)nuclei ratios is shown in Fig. 4. It provides the quality of the fit $\chi^2/ndf \simeq 8.04/10 \simeq 0.8$.

As one can see from Fig. 4, due to an exclusion of (anti)nuclei data from the IST EOS fit, the ratios $\frac{p}{\pi^+}$ and $\frac{\Xi^+}{\pi^+}$ are described slightly better compared to the MHRGM, while the relative deviation of the ratio $\frac{\Omega^+}{\pi^+}$ decreased from the MHRGM value 1 to the IST EOS value 0.5. Although the ratio $\frac{K^+}{\pi^+}$ is better reproduced by the MHRGM, the quality of description of all other ratios shown in Figs. 3 and 4 is almost the same.

4 Analysis of applicability range of various HRGM

In the work [8] the fit of the ALICE data led to finding out of a second minimum of χ^2/ndf at the CFO temperature of 274 MeV. Therefore, here we would like to study the behavior of $\chi^2(T_{CFO})/ndf$ up to $T_{CFO} = 600$ MeV, but simultaneously we would like to determine the applicability range of each version of HRGM discussed above. Such a study is necessary because it is hard to believe that at so high densities provided by the temperature 274 MeV the chemical freeze-out can occur.

The results of the fit with and without the light (anti)nuclei ratios are shown in Fig. 5 and are summarized in Table 3. From Fig. 5 one can see that the MHRGM and the IST EOS have a single minimum of $\chi^2(T)/ndf$ for $T \leq 600$ MeV. These findings are in line with the results of the recent ALICE data analysis [24], although our values of $\min\{\chi^2(T)/ndf\}$ are somewhat smaller. Moreover, as one can see from Table

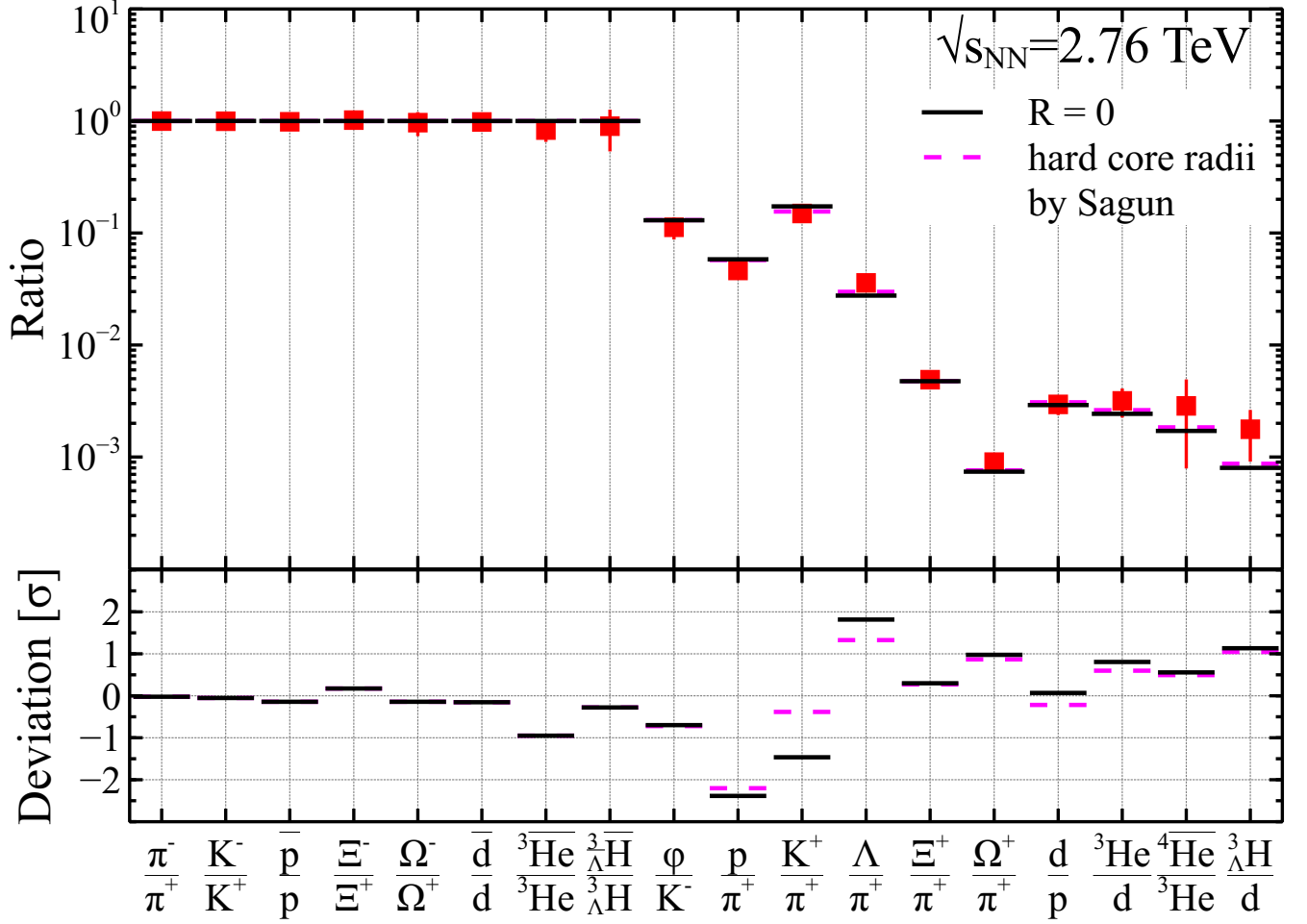


Figure 3: The full set of ALICE data (see Table 2) was fitted by the MHRGM with the hard-core radii taken from Ref. [5] with the CFO temperature $T_{CFO} \simeq 153 \pm 7$ MeV and $\chi^2/ndf \simeq 10.9/17 \simeq 0.64$. For a comparison the ideal gas fit results are also shown which correspond to $T_{CFO} \simeq 152 \pm 7$ MeV and $\chi^2/ndf \simeq 14.8/17 \simeq 0.87$. The upper panel shows the fit of the ratios, while the lower panel shows the deviation between data and theory in units of estimated error.

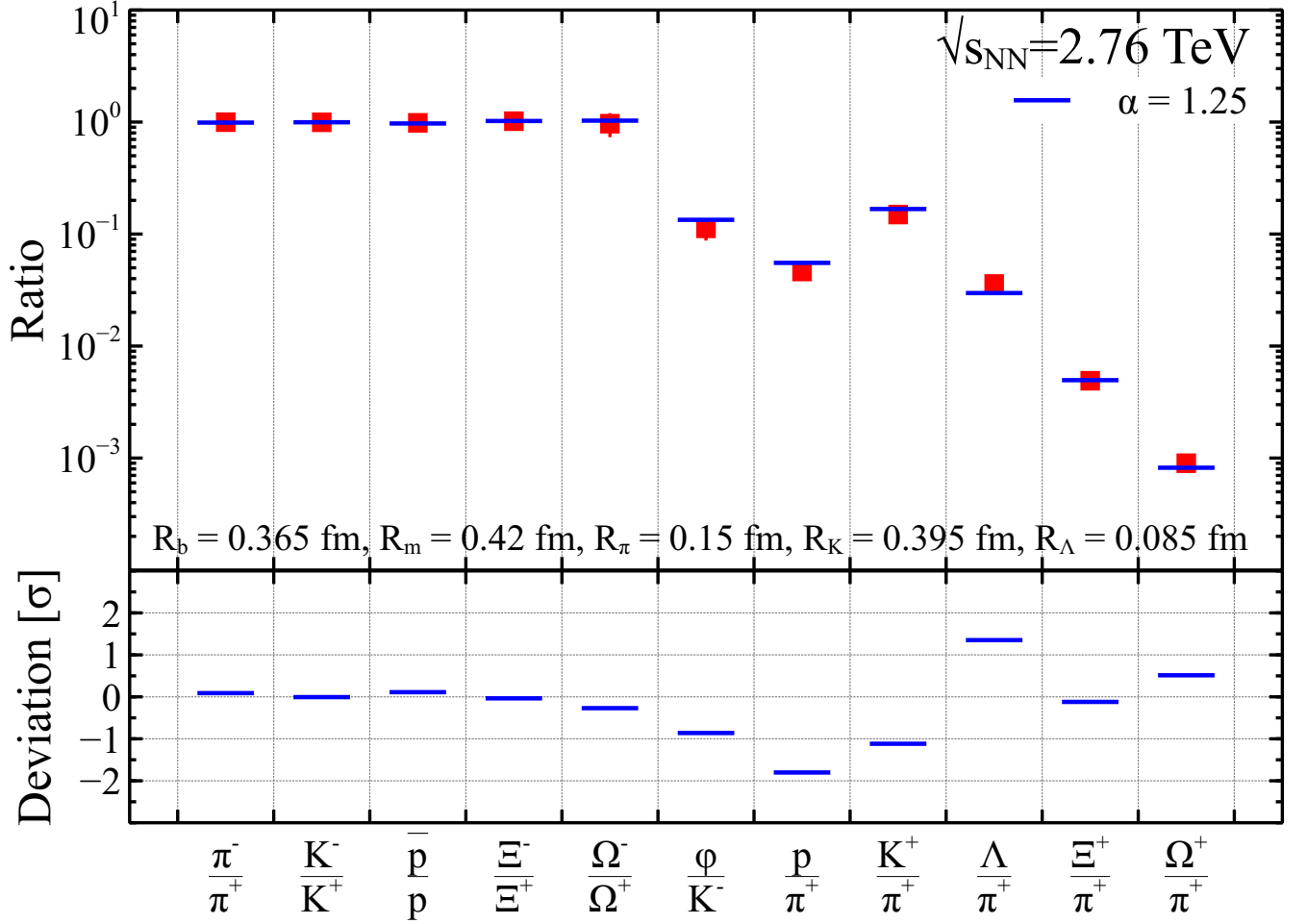


Figure 4: Same as in Fig. 3, but the fit was obtained by the IST EOS with the new hard-core radii found in Ref. [21]. The obtained CFO temperature is $T_{CFO} \simeq 152 \pm 7$ MeV. The (anti)nuclei ratios are not included in the fit and its quality is $\chi^2/ndf \simeq 8.04/10 \simeq 0.8$. The upper panel shows the fit of the ratios, while the lower panel shows the deviation between data and theory in units of estimated error.

3 the CFO temperatures of all found minima agree with each other very well. This means that the value of CFO temperature is defined by the hadronic ratios.

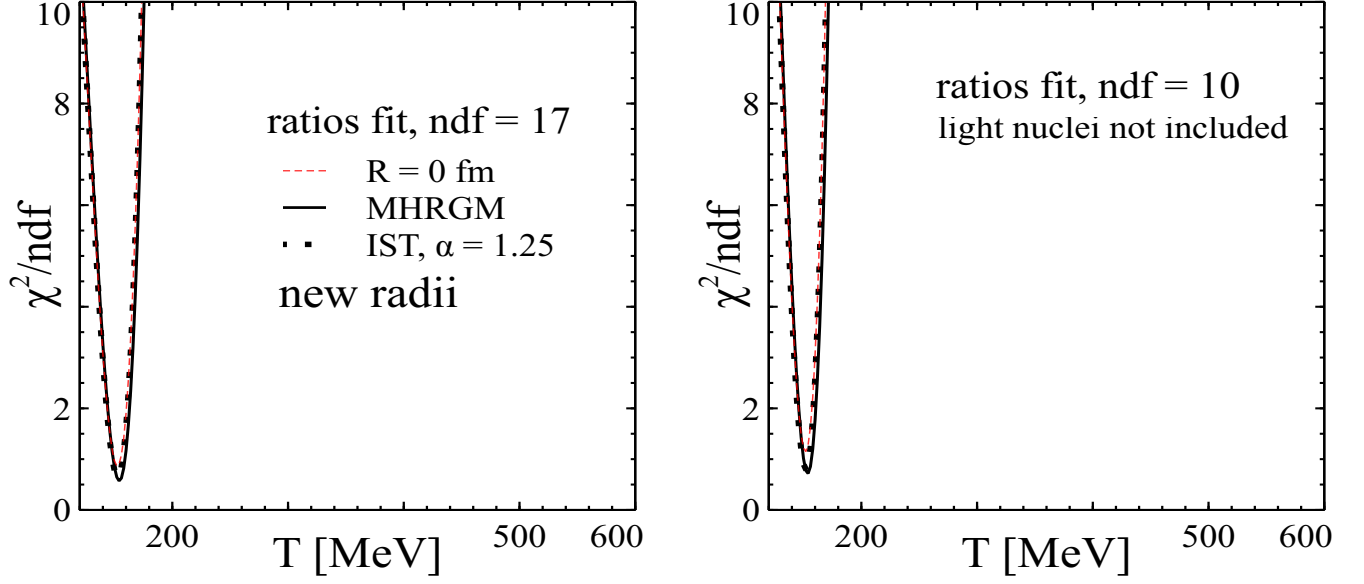


Figure 5: Comparison of the fit quality as a function of CFO temperature obtained for the new hard-core radii of Ref. [21] with the MHRGM (solid curve) and with IST EOS (dotted curve). The values of new hard-core radii are given in Fig. 4. Also the results of the fit with the vanishing hard-core radii of all hadrons are shown by the dashed curve. The left panel shows the results of fit in which the hadron yield ratios and the ones of light (anti)nuclei are taken into account, while in the right panel only the hadron ratios are fitted.

Next we study the applicability of various versions of the HRGM at high temperatures. For this purpose we employ the multi-component version of the Carnahan-Starling EOS known as the Mansoori-Carnahan-Starling-Leland (MCSL) EOS [25]. This EOS is well known in the theory of simple liquids [26] and has many applications in the statistical mechanics of polydisperse systems (see, for instance, Refs. [27, 28] and references therein). Similarly to the one-component case [16] the MCSL EOS accurately reproduces the pressure of hard spheres until packing-fraction values $\eta \leq 0.35 - 0.4$ [25, 27]. Here the packing fraction of the N -component mixture is defined in a standard way $\eta \equiv \sum_{k=1}^N \frac{4}{3} \pi R_k^3 \rho_k$ via the set of hard-core radii $\{R_k\}$ and the corresponding particle densities $\{\rho_k\}$. In terms of these notations the MCSL pressure [25] reads

$$p^{CS} = \frac{6T}{\pi} \left[\frac{\xi_0}{1 - \xi_3} + \frac{3\xi_1\xi_2}{(1 - \xi_3)^2} + \frac{3\xi_2^3}{(1 - \xi_3)^3} - \frac{\xi_3\xi_2^3}{(1 - \xi_3)^3} \right], \quad (11)$$

$$\xi_n = \frac{\pi}{6} \sum_{k=1}^N \rho_k [2R_k]^n. \quad (12)$$

Using Eqs. (11) and (12) we can determine the applicability bounds of any version of the HRGM by comparing its pressure with the MCSL pressure (11) found for the same value of temperature and for the same set of particle densities $\{\rho_k\}$. The results for the compressibility $Z = p/(\rho T)$ of the MHRGM are depicted in Fig. 6. Here the total pressure of the system is p , while the total particle density is $\rho = \sum_{k=1}^N \rho_k$.

In the left panel of Fig. 6 we present a comparison for the new set of radii, while its right panel shows the results for the Vovchenko-Stoecker (VS) [8] or the Bag model prescription for the hard-core radii

$$R_k = R_0 \left[\frac{m_k}{m_0} \right]^{\frac{1}{3}}, \quad (13)$$

Ndf	Model	T_{CFO} (MeV) at $\min\{\chi^2/ndf\}$	$\min\{\chi^2/ndf\}$
17	Ideal gas	152 ± 7	$\frac{14.78}{17} \simeq 0.87$
	MHRGM	154 ± 7	$\frac{9.71}{17} \simeq 0.57$
	IST EOS	152 ± 7	$\frac{11.32}{17} \simeq 0.67$
10	Ideal gas	152 ± 7	$\frac{11.49}{10} \simeq 1.15$
	MHRGM	154 ± 7	$\frac{7.16}{10} \simeq 0.72$
	IST EOS	152 ± 7	$\frac{8.04}{10} \simeq 0.8$

Table 3: Parameters of χ^2/ndf minima for different versions of the HRGM found for the new set of hard-core radii. The first column specifies the number of ratios used in the fit, the second column defines the HRGM, the third column gives the CFO temperature at the χ^2/ndf minimum, whereas the last column gives the value of χ^2/ndf at the minimum.

where the constants are, respectively, the hard-core radius $R_0 = 0.5$ fm and the mass $m_0 = 938$ MeV of the proton [8]. In contrast to all previous findings such a parameterization led the authors of Ref. [8] to the conclusion about existence of a deeper minimum of χ^2/ndf at very high temperature $T \simeq 274$ MeV where, according to present knowledge, the hadron gas does no longer exist. Leaving aside the questions whether the prescription (13) can, in principle, be applied to hadrons and how the CFO can occur at such a high temperature, we would like to determine whether the χ^2/ndf minimum at high temperatures is an artifact of the EVM or it, indeed, has some physical meaning.

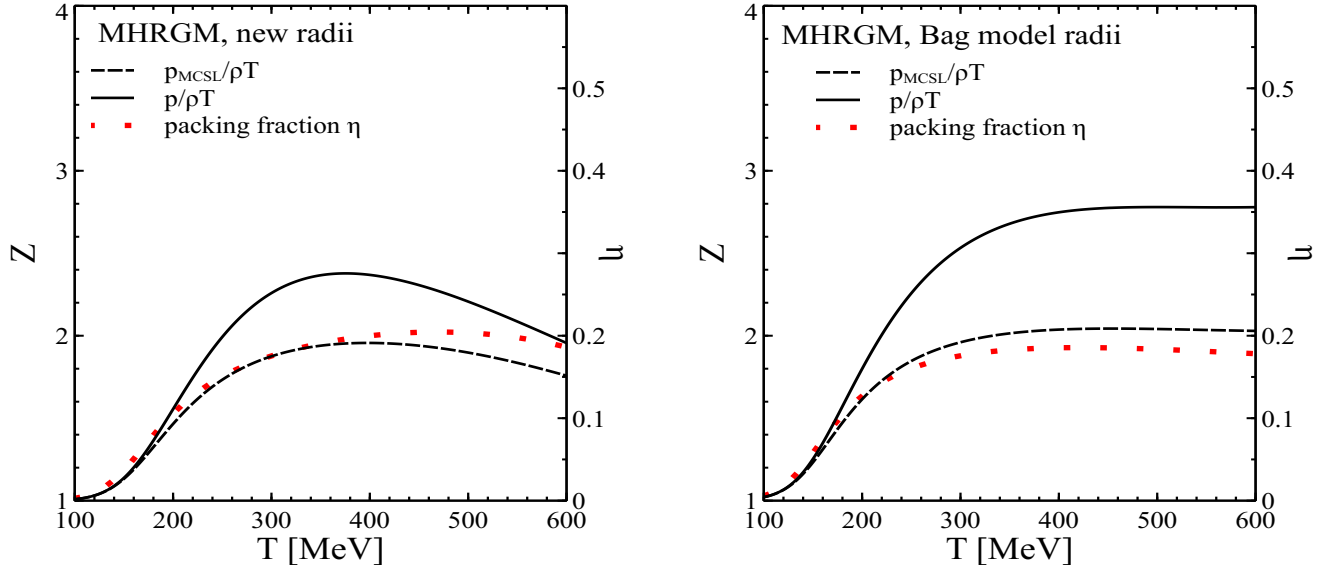


Figure 6: Thermal compressibility Z as a function of CFO temperature T is shown for the MHRGM and for the MCSL EOS. Z are found for the same particle densities. **Left panel:** the MHRGM (solid curve) and the MCSL EOS (dashed curve) results are obtained for the new set of hard-core radii [21]. The dotted curve demonstrates the CFO temperature dependence of the packing fraction. **Right panel:** same as in the left panel, but the VS prescription of Eq. (13) (solid curve) is compared with the MCSL EOS (dashed curve) for the same particle densities.

Based on the above discussion of the EVM applicability (see Sec. 2), we defined it by the inequality $\eta \leq 0.11$ for the packing fraction η . This condition defines the applicability temperature $T_{appl} \simeq 200$ MeV

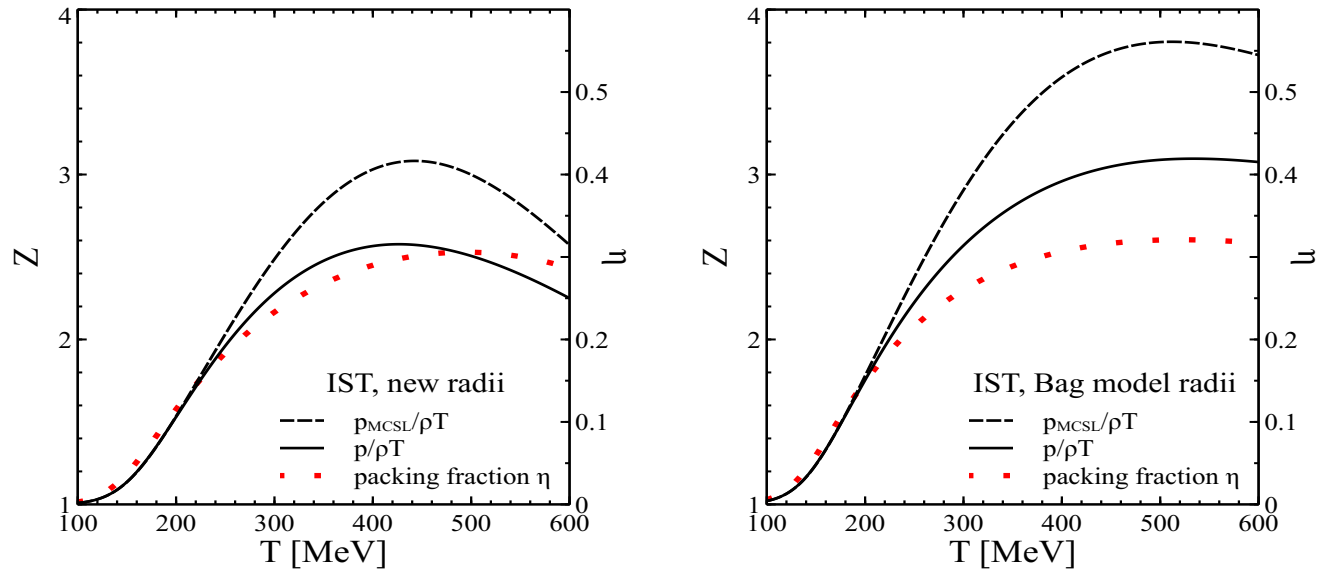


Figure 7: **Left panel:** Same as in Fig. 6, but for the IST EOS with the new hard-core radii found in Ref. [21]. **Right panel:** Same as in Fig. 6, but for the IST EOS with the VS prescription (13) for the hard-core radii.

for the MHRGM with the new radii (see the left panel of Fig. 6) and $T_{appl} \simeq 180$ MeV for the VS model (see the right panel of Fig. 6). Note that such an inequality corresponds to about 6% of relative deviation between the compressibility factor Z of the MHRGM and the one of the MCSL EOS. In other words, the inequality $\eta \leq 0.11$ is not too strict constraint on the applicability bounds of the MHRGM.

Also we would like to point out that for $\eta \geq 0.175$ the both versions of MHRGM whose packing fractions are shown in Fig. 6 become acausal, i.e. their speed of sound exceeds the speed of light. This finding is similar to the result of VS model reported in [8]. Thus, the causality condition provides a less strict constraint on the applicability bounds.

A similar investigation we performed for the IST EOS with the new set of hard-core radii and with the VS hard-core radii (13). The results are shown in Fig. 7. Since the IST EOS is valid for the packing fractions obeying inequality $\eta \leq 0.22$, we use this condition to determine the applicability temperature of this EOS. Using it we found that $T_{appl} \simeq 275$ MeV for the IST EOS with the new hard-core radii, while for the IST EOS with the VS hard-core radii we got $T_{appl} \simeq 235$ MeV. Note that these values of the applicability temperatures provide about 5% of relative deviation between the compressibility factor Z of the IST EOS and the one of the MCSL EOS, i.e. a constraint $\eta \leq 0.22$ is not too strict for the IST EOS.

From this analysis we can conclude that the minima of χ^2/ndf of the MHRGM and the ones of the IST EOS shown in Fig. 5 are located well inside the applicability bounds of these models.

5 Discussion of the results

Now we are ready to apply the IST EOS to the description of the ALICE data with the VS prescription for hard-core radii. For such a study we extended the MHRGM [2, 3, 5, 4] to the VS prescription (13) and fitted the ratios of hadron multiplicities. In other words, using Eq. (13) we calculate the second virial coefficient between the particles k and l with the hard-core repulsion as usual $b_{kl} = \frac{2\pi}{3}(R_k + R_l)^3$.

The obtained results are presented in Fig. 8. This figure shows the CFO temperature dependence of the fit quality χ^2/ndf . In this fit we used the same parameters in Eq. (13) as in Ref. [8]. From Fig. 8 one can see that the VS prescription for hard-core radii always generates the second minimum of χ^2/ndf at high temperatures. The parameters of all minima shown in Fig. 8 are given in Table 4.

We confirm the finding of Ref. [8] that the minima of the VS prescription (13) are strongly asymmetric

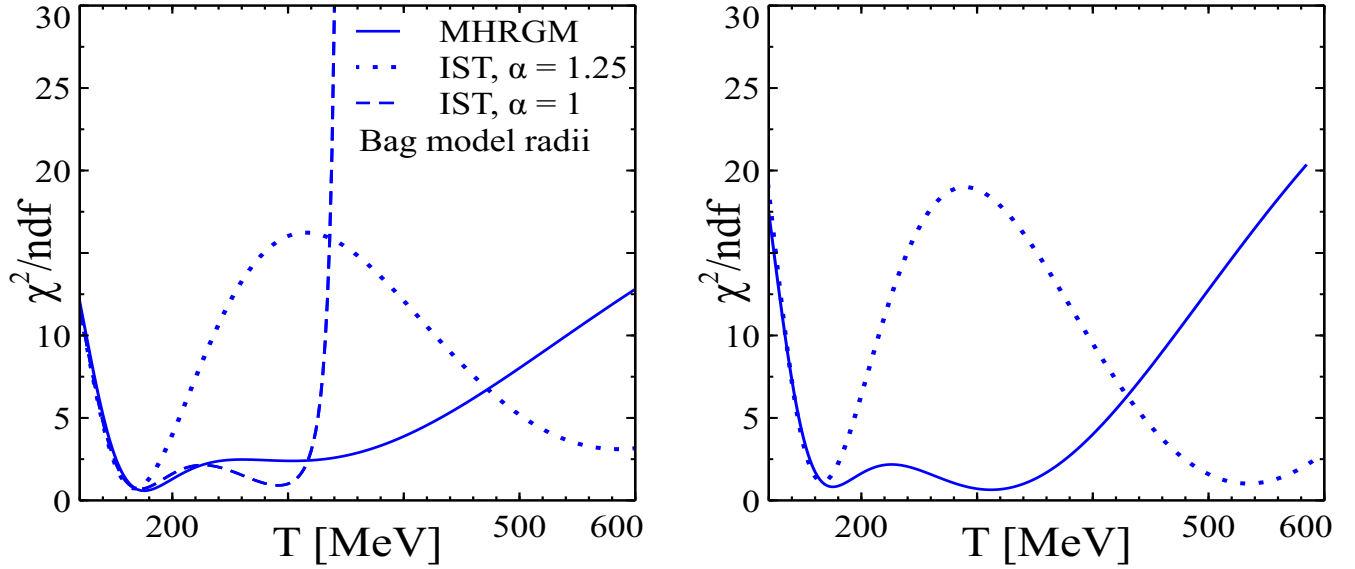


Figure 8: The fit quality as a function of CFO temperature for the MHRGM (solid curve), IST EOS with $\alpha = 1.25$ (dotted curve) and IST EOS with $\alpha = 1$ (dashed curve). All models employ the VS prescription of Eq. (13) for hard-core radii. Left panel shows the results for the light (anti)nuclei ratios included into the fit, while the results shown in right panel do not include these ratios. Note that for $T \leq 230$ MeV the solid and long dashed curves are hardly distinguishable because these are EVM.

for the MHRGM. The same is true for the IST EOS with $\alpha = 1$, which, as we discussed in Sec. 2, is also the EVM. This statement becomes apparent from the left panel of Fig. 7, if one compares the temperature dependence of solid and dashed curves in this figure. On the other hand, the IST EOS with $\alpha = 1.25$ demonstrates essentially different T -behavior (see below) and the asymmetry of its minima is less pronounced. Also the CFO temperatures of the first χ^2/ndf minimum (see the third column in Table 4) are shifted to higher temperatures 166-176 MeV compared to the case of the fixed hard-core radii. This is also in line with Ref. [8] results for the MHRGM.

As one can see from Table 4, if the light (anti)nuclei are included into a fit, the minimum at higher temperature is shallower, whereas, if they are not included, the minimum at higher temperature is slightly deeper. This is similar to the results of Ref. [8] for the MHRGM. However, the main differences between the results of the EVM and the IST EOS are as:

- (i) the high T minimum is shifted to temperatures above 500 MeV at which, according to the present days paradigm, one cannot use the hadronic language at all and the CFO concept does not make any sense, since the inelastic reactions at these temperatures are not frozen;
- (ii) in contrast to the EVM results, the two minima of the IST EOS χ^2/ndf are separated by a huge maximum.

Therefore, the expectations of the authors of Ref. [8], that the more elaborate models will confirm their statement that the CFO may occur in the temperature range 170-320 MeV, are not supported by our results. Moreover, comparing the applicability temperature $T_{appl} \simeq 235$ MeV of the IST EOS which employed the VS prescription with the temperatures of the χ^2/ndf second minimum (see the fifth column in Table 4), we conclude that none of the considered models can be applied at the temperatures at which the second minimum is found. Hence, we do not think it makes any sense to owe any physical meaning to these high temperature minima. Our second major conclusion is that the second minimum found in Ref. [8] at $T \simeq 274$ MeV and observed here in the EVM at $T \simeq 292 - 312$ MeV are artifacts of extrapolating the EVM with the VS prescription (13) for hard-core radii far beyond the limit of its applicability.

An apparent reason of the EVM failure at temperatures above 200 MeV is that it overestimates the third and higher virial coefficients compared to a more elaborate MCSL EOS and the IST EOS (the third and

Ndf	Model	T_{CFO}^{low} (MeV) at $\min\{\chi^2/ndf\}$	$\min\{\chi^2/ndf\}$	T_{CFO}^{high} (MeV) at $\min\{\chi^2/ndf\}$	$\min\{\chi^2/ndf\}$
17	MHRGM	176_{-18}^{+30}	$\frac{9.92}{17} \simeq 0.58$	304_{-43}^{+78}	$\frac{40.71}{17} \simeq 2.4$
	IST EOS ($\alpha = 1$)	172_{-19}^{+30}	$\frac{11.78}{17} \simeq 0.69$	292_{-46}^{+21}	$\frac{15.48}{17} \simeq 0.91$
	IST EOS	168 ± 14	$\frac{12.36}{17} \simeq 0.72$	586 ± 60	$\frac{52.82}{17} \simeq 3.1$
10	MHRGM	176_{-17}^{+30}	$\frac{8.21}{10} \simeq 0.82$	312_{-54}^{+46}	$\frac{6.44}{10} \simeq 0.64$
	IST EOS	166_{-13}^{+14}	$\frac{10.13}{10} \simeq 1.01$	534_{-48}^{+52}	$\frac{9.18}{10} \simeq 0.92$

Table 4: Parameters of χ^2/ndf minima for different versions of the HRGM found for the VS hard-core radii. The first, second, third and fourth columns have the same meaning as the ones in Table 3. The fifth column gives the CFO temperature at the second minimum of χ^2/ndf , and the last column gives the value of χ^2/ndf at this minimum.

fourth virial coefficients of the one component IST EOS can be found in [29]). Furthermore, it is clear that at high temperatures one cannot ignore the Lorentz contraction of the hard spheres [30, 31, 32, 33], since the existence of hard spheres is in contradiction with the postulates of relativity. Therefore, strictly speaking, all results of the EVM which are shown in Fig. 6 cannot be considered as trustworthy at temperatures above 200 MeV [30]. The effect of Lorentz contraction leads to a decreasing of the mean hard-core radius with the temperature, but for temperatures obeying the inequality $m_h < T < 2m_h$ (here m_h is the mass of hadron) the mean hard-core radius of a hadron is $2^{\frac{1}{3}} \simeq 1.26$ times smaller than the one at vanishing temperature [30]. Such a decrease corresponds to an about 50% reduction of the excluded volume of two identical non-relativistic hard spheres [30]. In other words, within the EVM for $T \sim 250$ MeV one has to account for the reduction of the hard-core radii of pions, kaons, and η meson, while for $T \sim 350$ MeV one should in addition account for such a reduction of the ω and ρ mesons' hard-core radii etc.

A principally different situation occurs for the IST EOS with $\alpha = 1.25$ and with the fixed hard-core radii of hadrons, since it correctly reproduces the MSCL EOS at those temperatures where the EVM fails, as one can see from the left panel of Fig. 7. Employing the new hard-core radii in the IST EOS, one finds that this EOS provides not more than a 5% deviation from the MSCL EOS at $T \leq T_{appl} \simeq 275$ MeV, i.e., in the region where the second minimum of the VS model was found in [8]. From the discussion given in Sec. 2 it is clear that the IST EOS accounts for the gradual decrease of the excluded volume of hadrons when the pressure increases. In principle, one should not consider the temperatures above T_{appl} , but let us discuss what will happen at higher temperatures. As one can see from the left panel of Fig. 7, at $T \simeq 340 - 350$ MeV the regime of the proper volume is reached by almost all hadrons and, hence, the packing fraction saturates at the value $\eta \simeq 0.3$. Accounting for this fact and remembering that the pion hard-core radius $R_\pi = 0.15$ fm is almost three times smaller than the hard-core radii of other mesons (hence the pion proper volume is about 25 times smaller than the proper volume of other mesons), we conclude: (i) at such temperatures the pions behave almost as point-like particles; (ii) the excluded volumes of other hadrons are now reduced to their proper volumes which are small. For instance, the proper volume of all baryons V_b^{new} , except the Λ -hyperons, is about $V_b^{new} \simeq 0.2$ fm³. Hence, accounting for the relativistic effects of a few species (kaons, η , ω and ρ mesons etc.) will stronger approximate the hadronic pressure to the one of ideal gas, which does not generate the second minimum at high temperatures. Thus, the Lorentz contraction effect cannot strongly affect the results of the IST EOS with the fixed values of hard-core radii [21].

Using the VS prescription (13) within the IST EOS we found its applicability temperature T_{appl} which provides not more than a 5% deviation from the MSCL EOS at $T_{appl} \simeq 235$ MeV. Note that the latter temperature is far below the region in which the authors of Ref. [8] found the second minimum of $\chi^2/ndf(T)$ and, hence, at this point one could stop any discussion of this issue. Moreover, according to the lattice

QCD one cannot use the hadronic language at temperatures above 160-170 MeV at any baryonic density and, therefore, we do not have to discuss the VS prescription further. However, let us see what will happen, if one follows the logic of Refs. [8, 34] insisting on the fact that the IST EOS with the VS hard-core radii provides a better description of the present ALICE data at the CFO temperatures above 500 MeV. In this case at $T \geq 500$ MeV only pions, η -mesons and kaons will behave as the ideal gas, whereas all heavier hadrons will have rather large proper volumes. For instance, for the proton radius $R_0 = 0.5$ fm used in [8] the nucleon proper volume V_p^{VS} in the VS model is $V_p^{VS} \simeq 0.52 \text{ fm}^3$ which is essentially larger than the proper volume of baryons V_b^{new} found for the set of new hard-core radii [21]. Therefore, for nucleons and heavier hadrons one will have to include the Lorentz contraction of the VS hard-core radii.

Note that at $T = 500$ MeV the nucleon proper volume V_p^{VS} is reduced to about $0.65 V_p^{VS} \simeq 0.34 \text{ fm}^3$ due to the Lorentz contraction [31]. Similarly, the effect of induced surface tension of nucleons and heavier hadrons will weaken and, hence, the number of all these hadrons will be sizably enhanced due to high pressure. Using the qualitative explanation of the fact that decreasing the hard-core radius of nucleons, one increases the temperature of the second minimum of χ^2/ndf for the ALICE data [34, 35], we conclude that inclusion of the Lorentz contraction into the IST EOS with VS radii will inevitably shift the second minimum to even higher temperatures which may not be achieved by the initially thermalized state formed in relativistic heavy-ion collisions. In other words, in this section it is shown that the location of a minimum at high temperatures depends on the degree of model refinement. Then our final conclusion is that the additional minimum, found in Ref. [8], is unphysical.

6 Conclusions

In this work we developed a novel formulation of the HRGM, the so-called induced surface tension EOS (IST EOS), which explicitly accounts for the surface tension induced by the interaction between particles. Such an approach was developed earlier in Ref. [17] on the basis of the virial expansion for an N -component mixture of gases which have individual hard-core radii. Using the freedom of the Van der Waals extrapolation to high particle densities we introduced a parameter α , which here is found to serve as a “switch” between the excluded and proper volume regimes. A detailed comparison with the famous Carnahan-Starling EOS demonstrates the validity of the IST EOS at higher packing fractions 0.2-0.22 than the traditional EVM, which is valid up to packing fractions of about 0.1-0.11. Moreover, we found that the IST EOS is softer than the Carnahan-Starling EOS [16] and its multi-component version MCSL EOS [25]; as a result, the model respects causality up to higher densities than these famous EOS.

Here we constructed the particle-yield ratios from the multiplicities measured by the ALICE experiment at $\sqrt{s_{NN}} = 2.76$ TeV, which we fitted to the different versions of the HRGM, namely the EVM and IST EOS. It is found that the MHRGM and IST EOS provide almost the same high fit quality with $\chi^2/ndf \simeq 0.6 - 0.8$ and practically the same value of the CFO temperature $T_{CFO} \simeq 154 \pm 7$ MeV. In addition, within the MHRGM we analyzed the VS model with the bag-like prescription (13) for the hard-core radii. Due to a different realization of the Van der Waals repulsion in our analysis of the VS prescription (13) we found a second minimum of χ^2/ndf at slightly higher temperatures $T = 292 - 312$ MeV compared to the work [8]. Also we showed that the MHRGM with the VS prescription (13) for hard-core radii cannot be applied at temperatures above $T \simeq 180$ MeV, since it gets stiffer than the non-relativistic mixture of hard spheres. An apparent consequence is that its speed of sound exceeds the speed of light at high temperatures, which makes the whole treatment unphysical.

Using the IST EOS we performed the fit of ALICE data with fixed values of hard-core radii for pions, kaons, Λ (anti)hyperons, other mesons, and other baryons and found no traces of the high-temperature minimum for $T_{CFO} \leq 600$ MeV, although such a model, as we showed here, is applicable at temperatures below 275 MeV. Furthermore, to get rid of any suspicions about existence of the high-temperature minimum for the VS prescription (13), we analyzed the ALICE data with the IST EOS using hard-core radii given by Eq. (13). Although such an EOS is applicable at temperatures below 235 MeV only, we did not see any additional minimum within this range of temperatures, whereas we again found a second minimum at a temperature above 500 MeV, i.e., where the IST EOS is inapplicable. Therefore, we showed that the

high-temperature minimum of χ^2/ndf found in Ref. [8] and further discussed in [34] is a consequence of extrapolating the Van der Waals EOS far beyond the limits of its applicability.

Acknowledgments. The authors are thankful to A. Andronic, D. B. Blaschke, P. Braun-Munzinger, T. Galatyuk, C. Greiner, and M. Gazdzicki for fruitful discussions and for important comments. We thank V. Vovchenko for the constructive criticism, comparison to his results and important corrections. The authors give their cordial thanks to D. R. Oliinychenko for a thorough verification of fitting results, for very important critical comments and for a suggestion to present the packing fraction in the figures 6 and 7. We thank D. H. Rischke for a critical reading of the manuscript. K.A.B., V.V.S., A.I.I. and G.M.Z. acknowledge a partial support from the program “Nuclear matter under extreme conditions” launched by the Section of Nuclear Physics of NAS of Ukraine. K.A.B. acknowledges a partial support by the ExtreMe Matter Institute EMMI, GSI Helmholtzzentrum für Schwerionenforschung, Darmstadt, Germany.

7 Appendix: Expression for particle density

In order to compare the IST EOS with the generalized Carnahan-Starling EOS [25] we need to have the explicit expressions for the particle density of hadrons of species k . Here we consider the generalized system (1) and (2), i.e., the partial pressure p_k and the partial surface-tension coefficient Σ_k are defined as

$$p_k = T\phi_k \exp \left[\frac{\mu_k}{T} - \frac{4}{3}\pi R_k^3 \frac{p}{T} - 4\pi R_k^2 \frac{\Sigma}{T} \right], \quad (14)$$

$$\Sigma_k = T R_k \phi_k \exp \left[\frac{\mu_k}{T} - \frac{4}{3}\pi R_k^3 \frac{p}{T} - 4\pi R_k^2 \alpha_k \frac{\Sigma}{T} \right] \equiv p_k R_k \exp \left[-4\pi R_k^2 (\alpha_k - 1) \frac{\Sigma}{T} \right], \quad (15)$$

where the total chemical potential is given by Eq. (3). Then the total pressure and the total surface-tension coefficient are defined as $p = \sum_k p_k$ and $\Sigma = \sum_k \Sigma_k$, respectively. The system (14) and (15) is a generalization of Eqs. (1) and (2) to the case when each particle species has its own value of the parameter α_k . Evidently, setting $\alpha_1 = \alpha_2 = \dots = \alpha_k = \dots = \alpha$ in Eqs. (14) and (15) one obtains Eqs. (1) and (2).

Differentiating p and Σ with respect to the full chemical potential μ_k of the hadron of sort k one finds

$$\begin{pmatrix} a_{11} & a_{12} \\ a_{21} & a_{22} \end{pmatrix} \cdot \begin{pmatrix} \frac{\partial p}{\partial \mu_k} \\ \frac{\partial \Sigma}{\partial \mu_k} \end{pmatrix} = \begin{pmatrix} \frac{p_k}{T} \\ \frac{\Sigma_k}{T} \end{pmatrix} \quad (16)$$

Here the coefficients a_{kl} can be expressed in terms of the partial pressures $\{p_k\}$ and the partial surface-tension coefficients $\{\Sigma_k\}$ as

$$a_{11} = 1 + \frac{4}{3}\pi \sum_k R_k^3 \frac{p_k}{T}, \quad (17)$$

$$a_{12} = 4\pi \sum_k R_k^2 \frac{p_k}{T}, \quad (18)$$

$$a_{21} = \frac{4}{3}\pi \sum_k R_k^3 \frac{\Sigma_k}{T}, \quad (19)$$

$$a_{22} = 1 + 4\pi \sum_k R_k^2 \alpha_k \frac{\Sigma_k}{T}. \quad (20)$$

Then the particle density of hadrons of species k is given by

$$\rho_k \equiv \frac{\partial p}{\partial \mu_k} = \frac{1}{T} \cdot \frac{p_k a_{22} - \Sigma_k a_{12}}{a_{11} a_{22} - a_{12} a_{21}}. \quad (21)$$

The charge density of kind A ($A \in \{B, S, I_3\}$) of a hadron of species k can be found by multiplying Eq. (21) by the partial derivative $\frac{\partial \mu_k}{\partial \mu_A} = A_k$.

References

- [1] A. Andronic, P. Braun-Munzinger and J. Stachel, Nucl. Phys. A **772**, 167 (2006) and references therein.
- [2] K. A. Bugaev, D. R. Oliinychenko, A. S. Sorin and G. M. Zinovjev, Eur. Phys. J. A **49**, 30 (2013).
- [3] K. A. Bugaev et al., Europhys. Lett. **104**, 22002 (2013).
- [4] K. A. Bugaev et al., Phys. Part. Nucl. Lett. **12**, 351 (2015).
- [5] V. V. Sagun, Ukr. J. Phys. **59**, 755 (2014).
- [6] S. Chatterjee, R. M. Godbole and S. Gupta, Phys. Lett. B **727**, 554 (2013).
- [7] K. A. Bugaev et al., Eur. Phys. J. A **52**, 175 (2016).
- [8] V. Vovchenko and H. Stöcker, arXiv:1512.08046v2 [hep-ph].
- [9] B. Abelev *et al.* [ALICE Collaboration], Phys. Rev. C **88**, 044910 (2013).
- [10] B. B. Abelev *et al.* [ALICE Collaboration], Phys. Lett. B **728**, 216 (2014); Erratum: [Phys. Lett. B **734**, 409 (2014)]
- [11] B. B. Abelev *et al.* [ALICE Collaboration], Phys. Rev. Lett. **111**, 222301 (2013).
- [12] A. G. Knospe [ALICE Collaboration], J. Phys. Conf. Ser. **509**, 012087 (2014).
- [13] J. Adam *et al.* [ALICE Collaboration], Phys. Rev. C **93**, 024917 (2016).
- [14] B. Dönigus [ALICE Collaboration], EPJ Web Conf. **97**, 00013 (2015).
- [15] J. Adam *et al.* [ALICE Collaboration], Phys. Lett. B **754**, 360 (2016).
- [16] N. F. Carnahan and K. E. Starling, J. Chem. Phys. **51**, 635 (1969).
- [17] V. V. Sagun, K. A. Bugaev, A. I. Ivanytskyi, I. N. Mishustin, Nucl. Phys. A, **924**, 24 (2014).
- [18] S. Das Gupta and A. Z. Mekjian, Phys. Rev. C **57**, 1361 (1998).
- [19] L. M. Satarov, K. A. Bugaev and I. N. Mishustin, Phys. Rev. C **91**, 055203 (2015).
- [20] J. Rafelski, Phys. Lett. B **62**, 333 (1991).
- [21] V. V. Sagun et al., Hadron Resonance Gas Model with the Induced Surface Tension (in preparation).
- [22] J. Stachel, A. Andronic, P. Braun-Munzinger and K. Redlich, J. Phys. Conf. Ser. **509**, 012019 (2014).
- [23] J. R. Taylor, “*An introduction to error analysis*”, University Science Book Mill Valley, California (1982).
- [24] A. Andronic, P. Braun-Munzinger, K. Redlich and J. Stachel, arXiv:1611.01347 [nucl-th].
- [25] G. A. Mansoori, N. F. Carnahan, K. E. Starling and T. W. Leland, Jr., J. Chem. Phys. **54**, 1523 (1971).
- [26] J. P. Hansen and I. R. McDonald, “*Theory of simple liquids*”, Academic, London (2006).
- [27] J. J. Salacuse and G. Stell, J. Chem. Phys. **77**, 3714 (1982).
- [28] Y. S. Wei and R. J. Sadus, AIChE J. **46**, 169 (2000).

- [29] V. V. Sagun, K. A. Bugaiev, A. I. Ivanytskyi, D. R. Oliinychenko and I. N. Mishustin, arXiv:1611.07071 [nucl-th].
- [30] K. A. Bugaev, M. I. Gorenstein, H. Stöcker and W. Greiner, Phys. Lett. B **485**, 121 (2000) and references therein.
- [31] K. A. Bugaev, Nucl. Phys. A **807**, 251 (2008).
- [32] D. R. Oliinychenko, K. A. Bugaev and A. S. Sorin, Ukr. J. Phys. **58**, 211 (2013).
- [33] S. Typel, Eur. Phys. J. A **52**, 16 (2016) and references therein.
- [34] V. Vovchenko, M. I. Gorenstein, L. M. Satarov, and H. Stoecker, arXiv:1606.06350v1 [hep-ph].
- [35] L. M. Satarov, V. Vovchenko, P. Alba, M. I. Gorenstein and H. Stoecker, arXiv:1610.08753v1 [nucl-th].